



Rapid Fabrication of Hydrophobic/Hydrophilic Patterns on Paper Substrates for Paper Spray Mass Spectrometry

Journal:	<i>Analyst</i>
Manuscript ID	AN-ART-06-2023-001071.R1
Article Type:	Paper
Date Submitted by the Author:	06-Sep-2023
Complete List of Authors:	Arias, Austin; Furman University, Chemistry Windham, Peyton; Furman University, Chemistry Cheyne, Natalie; Furman University, Chemistry Gilliland, Mac; Furman University, Chemistry

1
2
3 **Title:** Rapid Fabrication of Hydrophobic/Hydrophilic Patterns on Paper Substrates for Paper
4 Spray Mass Spectrometry
5

6 **Authors:** Austin Arias*[†], Peyton E. Windham*[†], Natalie A. Cheyne[†], William M. Gilliland, Jr. [†]
7

8 *These authors contributed equally to this work.
9

10 [†]Department of Chemistry, Furman University, Greenville, SC 29613
11

12 **Abstract**

13

14 A simple, rapid chemical coating and patterning method was developed and optimized
15 for paper-based substrates for use in paper spray mass spectrometry (PS-MS). A variety of
16 chlorosilanes were explored for coating paper substrates, and their effectiveness in forming
17 hydrophobic surfaces was characterized via contact angle goniometry, scanning electron
18 microscopy, and energy dispersive x-ray spectroscopy. Trichloromethylsilane was selected as the
19 primary coating agent because of the short time required to produce a hydrophobic surface
20 (contact angle >130°), as well as the ease of patterning. Patterning was performed using 3D-
21 printed masks and an oxygen/plasma cleaner. Optimal mask thickness and oxygen/plasma
22 cleaning parameters were determined to produce channels varying from 0.5 to 2.5 mm in width.
23 The effectiveness of the patterned substrates for PS-MS was determined via analysis of four
24 antiretrovirals: emtricitabine, lamivudine, efavirenz, and dolutegravir. Calibration curves were
25 made for each antiretroviral at varying channel widths, and the limits of detection and limits of
26 quantification for each drug were determined. These results show that this patterning method
27 results in an average 7.2-fold improvement in sensitivity and an average 190-fold improvement
28 in limits of detection over uncoated paper substrates in a neat matrix. In a proof-of-concept
29 experiment, calibration curves were generated for each antiretroviral in urine. A patterned paper
30 substrate with a 2-mm channel resulted in an average 7.4-fold improvement in sensitivity and an
31 average 18-fold improvement in limits of detection over uncoated paper substrates.
32
33
34
35
36

37 **Introduction**

38

39 Ambient ionization mass spectrometry (MS) has emerged over the past two decades as a
40 powerful method for rapid detection of an analyte with minimal sample preparation.^{1,2} The
41 development of ambient ionization MS began with desorption electrospray ionization (DESI)^{3,4}
42 and direct analysis in real time (DART)⁵ and has since expanded to include a large number of
43 other techniques. Since its development in 2010, paper spray (PS) has become one of the most
44 widely used ambient ionization techniques.⁶ In a typical PS experiment, a sample is spotted on a
45 triangular paper substrate and allowed to dry, which is followed by the addition of a solvent and
46 application of high voltage, resulting in a spray from a corner of the paper that can be detected
47 by a mass spectrometer. In addition to rapid detection and simple operation, PS has the added
48 advantage of inexpensive operation, using only paper substrates, high voltage, and small
49 volumes of solvents. The benefits of PS-MS have led to its development for a range of
50 applications including forensics,⁷⁻¹¹ environmental monitoring,¹²⁻¹⁶ drug screening and clinical
51 diagnostics,¹⁷⁻²³ as well as reaction monitoring.²⁴⁻²⁸
52
53
54
55
56
57
58
59
60

1
2
3 An attractive feature of PS is the ability to enhance analysis by chemical or physical
4 modification of the paper substrate. One approach to paper modification is to imbue the paper
5 with particles, often using starch as an adhesive agent. Several groups have used this strategy to
6 coat paper substrates with polystyrene microspheres,^{29,30} zirconia,³¹ silica,^{32,33} nanoparticles,^{34,35}
7 and metal organic frameworks.^{36,37} Another common strategy for paper modification has been to
8 take advantage of the reactivity of surface hydroxyl groups and chemically functionalize the
9 surface. The goal of chemical coating has often been to produce a hydrophobic surface,^{11,38–40}
10 though several groups have also modified substrates with the goal of increasing specificity for a
11 range of targets including biomolecules and other polar compounds.^{41–43}
12
13
14

15 One modification to paper substrates for PS-MS that has improved analytical
16 performance is the introduction of hydrophilic channels surrounded by hydrophobic barriers to
17 direct the solvent toward the inlet. Without directing solvent flow, the solvent will spread
18 throughout the entirety of the substrate. Multiple groups have addressed this issue by creating
19 hydrophobic barriers from photoresist,⁴⁴ paraffin,⁴⁵ wax,⁴⁶ and combinations of the latter two.⁴⁷
20 Photoresists have been shown to increase background in the mass spectrometry signal, limiting
21 sensitivity via ion suppression, and paraffin and wax must be heated to fully penetrate the paper,
22 which may reduce dimensional control. In addition, Jackson, *et al.* noted in a recent paper that
23 the wax printer used for much of this work is now discontinued.⁴⁸ With the exception of
24 photoresist, there is a notable lack of published approaches to chemically pattern paper substrates
25 for PS-MS. A number of chemical patterning approaches have been developed for other
26 microfluidic paper-based analytical devices (μ PADs),^{49–51} but very few of these have been
27 applied to PS-MS.
28
29
30
31

32 Herein, a simple approach is introduced to chemically coat and pattern paper substrates
33 for PS-MS. Paper substrates are first chemically modified to become hydrophobic via reaction
34 with trichloromethylsilane (TCMS). Following coating, hydrophilic channels are created in the
35 substrates by controlled oxidation of the coating via 3D-printed masks and treatment by
36 oxygen/plasma. Channel geometry is varied to test sensitivity and limits of detection for a set of
37 antiretrovirals (ARVs) used to treat HIV in both methanol/water and urine.
38
39
40

41 **Experimental**

42 *Chemicals and Materials*

43
44 Methanol (LC-MS), water (LC-MS), formic acid (LC-MS), and hexane (reagent grade)
45 were obtained from Fisher Scientific (Pittsburgh, PA, USA). Whatman 1 filter paper (110 mm
46 diameter) and petri dishes (100 mm diameter) were also obtained from Fisher Scientific.
47 Trichloromethylsilane (TCMS), trichlorophenylsilane (TCPhS), trichlorooctylsilane (TCOS),
48 and trichloro-(3,3,3-trifluoropropyl)-silane (TCFS) were obtained from Sigma Aldrich (St.
49 Louis, MO, USA). L-Dopa, efavirenz (EFV), dolutegravir (DTG), emtricitabine (FTC), and
50 lamivudine (3TC) were also obtained from Sigma. The ARVs have the following C_{\max} values
51 from FDA drug label data: 4.1 $\mu\text{g/mL}$ (EFV), 3.7 $\mu\text{g/mL}$ (DTG), 1.8 $\mu\text{g/mL}$ (FTC), 1.4 $\mu\text{g/mL}$
52 (3TC).⁵² Pooled human urine was obtained from Innovative Research (Novi, MI, USA). Plastic
53 masks were designed in Solidworks 2020 (Solidworks Corporation, Waltham, MA, USA) and
54
55
56
57
58
59
60

1
2
3 sliced for 3D printing using PrusaSlicer (Prusa Research, Czech Republic). Prusament polylactic
4 acid (PLA) was used for all masks on a Prusa MK3S printer. Food coloring obtained from a local
5 grocery store was added to water to create a colored solution to view the channels on the paper
6 substrates.
7

8 9 *Coating and Patterning*

10 Filter paper substrates were cut into quarters prior to coating and placed in a petri dish,
11 with one to three quarter papers per dish. A volume of 15 mL of 5, 10, or 50 mM of each silane
12 in hexane was added to the petri dish with immersion times ranging from 5 to 120 minutes. The
13 papers were removed with tweezers and were hung to dry in a hood.
14
15

16 Coated papers were characterized via contact angle goniometry (CAG), scanning electron
17 microscopy (SEM), and energy-dispersive x-ray spectroscopy (EDS). CAG was performed with
18 a KSV Theta Optical Tensiometer. Contact angles were measured for 5 μL drops of deionized
19 water using Attention Theta software. A minimum of three replicates were collected for each
20 sample. SEM images and EDS spectra were acquired with a JEOL JSM-IT-200LA equipped
21 with a JEOL JED-2300 Dry SDD EDS detector.
22
23

24 For patterning optimization, papers were cut into rectangles (45 x 30 mm). For paper
25 spray substrates, the papers were cut into isosceles triangles (8 mm base x 16 mm height). The
26 paper substrates were then placed in 3D-printed PLA cartridges used as masks. The masks had
27 nominal channel widths of 0.5, 1.0, 1.5, 2.0, and 2.5 mm. The paper in the cartridge was then
28 exposed to oxygen/plasma using a plasma cleaner (PDC-32G, Harrick Plasma, Ithaca, NY) for 5
29 to 20 s set at low, medium, or high intensity. The chamber was evacuated to <0.2 Torr via a
30 roughing pump (IDP-3 dry scroll pump, Agilent Technologies, Santa Clara, CA, USA). Oxygen
31 gas (~ 200 Torr) was then added to the chamber via a needle valve. The valve to the oxygen was
32 closed, and the chamber was evacuated to <0.2 Torr. Oxygen (~ 1 Torr) was then added to the
33 chamber. The valve was closed once more, and the chamber was evacuated to <0.2 Torr. The RF
34 voltage was then turned on and set at the desired intensity. The valve to the oxygen was
35 reopened, creating a plasma in the chamber at a pressure of ~ 1 Torr. After the desired exposure
36 time, the voltage was turned off, and the chamber was vented to remove the samples. The papers
37 were removed from the cartridges and stored in petri dishes under ambient conditions until
38 further analysis.
39
40
41
42
43

44 *Paper Spray Mass Spectrometry*

45 For our initial tests, standard calibration solutions were prepared in 50/50 methanol/water
46 (v/v) at the following concentrations: 0 (blank), 10, 25, 50, 100, 250, 500, and 1250 ng/mL. Each
47 solution contained FTC, 3TC, EFV, and DTG plus L-Dopa as an internal standard at a
48 concentration of 250 ng/mL. A volume of 6 μL of each standard was spotted onto the center of
49 the paper substrates and allowed to dry before analysis. For urine samples, standard calibration
50 solutions with the four ARVs were prepared in urine at the following concentrations: 0 (blank),
51 100, 250, 500, 1250, 2500, and 5000 ng/mL, with each having L-Dopa as an internal standard at
52 500 ng/mL. A volume of 6 μL of urine was spotted onto the center of paper substrates and
53 allowed to dry prior to analysis.
54
55
56
57
58
59
60

All paper spray mass spectrometry experiments were performed with an LTQ Velos Pro Dual Ion Trap Mass Spectrometer (ThermoFisher Scientific, Waltham, MA). A voltage of +4 kV was applied for all experiments via a copper clip, held in place by a laboratory clamp. The spray solvent for all analyses was 50/50 methanol/water (v/v) spiked with 0.1% formic acid and was placed manually on the paper via micropipette. Prior to pipetting, the solvent was kept on ice during the analysis. Uncoated paper substrates required 20 μ L of solvent to sustain an electrospray for the period of analysis. The volume applied to patterned substrates depended on channel width, ranging from 5 μ L for the 0.5 mm wide channels to 8 μ L for the 2.5 mm wide channels. MS/MS transitions for each target analyte were as follows: m/z 420 \rightarrow m/z 277 (DTG), m/z 316 \rightarrow m/z 244 (EFV), m/z 248 \rightarrow m/z 130 (FTC), m/z 230 \rightarrow m/z 112 (3TC), and m/z 198 \rightarrow m/z 181 (L-Dopa). L-Dopa was chosen as a cost-effective internal standard. Data were acquired via a method in which the electrospray voltage was off for 0.1 min, turned on for 1.0 min, and then turned off for 0.1 min, creating a peak that could be integrated. The areas of the peaks for the analytes and internal standard were integrated using Freestyle Software (ThermoFisher Scientific).

Results and Discussion

Hydrophobic Coating

The initial approach for creating patterned paper was to first coat an entire paper with hydrophobic reagents, followed by controlled removal of a portion of the coating using a mask during oxygen/plasma exposure. The reaction of chlorosilanes with surface hydroxyl groups is well-established and robust, so we explored four chlorosilane reagents for surface modification: TCMS, TCOS, TCPhS, and TCFS. After each reaction, the hydrophobicities of the papers were measured via CAG. We tested a range of reagent concentrations and coating times, shown in **Figure 1**. Each data point represents an average of three contact angle measurements. Missing data points indicate that a contact angle was not measurable (i.e., the paper remained hydrophilic). Error bars were removed for graph readability. Papers modified with TCOS and TCMS showed consistently larger maximum contact angles than the other two silanes ($>\sim 130^\circ$), indicating a more hydrophobic surface. In addition, these two silanes produce a hydrophobic surface after just 5 minutes of coating. TCFS-modified papers showed consistent contact angles of $\sim 120^\circ$, with a higher concentration necessary to produce that contact angle at shorter times. TCPhS-modified paper substrates were overall the least hydrophobic and required 30 minutes for the contact angle to reach a maximum at the highest concentration (50 mM). Sample contact angle images for silane-modified paper are shown in **Figure 2**.

The morphology of the paper surfaces was characterized by scanning electron microscopy, and sample images for each type of modified paper are shown in **Figure 3**. The fibers of each of the coated papers are visible in the images, and the morphology of the coated papers is similar to that of the uncoated paper. Thus, the morphology observed by SEM suggests that the hydrophobicity of the paper is due to a thin layer of silanes. In the case of the TCMS-coated paper, there were small clumps of material visible on the surface that are not present on any of the other paper substrates, likely aggregates formed from polymerization of TCMS, creating a rougher surface than the other silanes. TCMS contains the simplest chain of the four

1
2
3 silane reagents (a methyl group), so it was expected that TCMS might produce the least
4 hydrophobic surface. Previous research has shown that both surface chemistry and roughness
5 play a role in hydrophobicity.⁵³ Thus, the observed images suggest that the hydrophobicity of the
6 TCMS-coated papers may be a combination of the modification of the surface and an increase in
7 surface roughness. Given the small size of the methyl group relative to the other silane side
8 chains (phenyl, trifluoropropyl, and octyl), there may be a denser coating of TCMS at the surface
9 due to reduced steric interaction of the side chains. Thus, increased hydrophobicity could also be
10 due to larger density of TCMS coating at the surface.
11
12

13
14 The presence of silicon on the papers was confirmed by energy dispersive X-ray
15 spectroscopy. The EDS spectra for each type of paper are shown below the corresponding SEM
16 images in **Figure 3**. Each of the EDS spectra contains carbon and oxygen peaks both from the
17 paper itself and the silane reagents. For the coated papers, each spectrum also has a silicon peak
18 that is not observed on uncoated paper, providing evidence for the presence of the desired
19 reaction product. In addition, a fluorine peak is observed for the TCFS-coated paper, providing
20 further evidence of successful surface modification. Taking into account optimal coating time
21 (~5 min), similarity of paper morphology to uncoated papers, and hydrophobicity of the paper
22 (>130° by CAG), TCMS and TCOS were chosen as the initial primary coating agents for the
23 paper substrates.
24
25

26 *Patterning*

27
28
29 In order to optimize the patterning parameters for different channel widths, we designed a
30 3D-printed mask with varying channel widths, shown in **Figure 4A**. The mask is made of orange
31 plastic (PLA), and the channels nominally ranged from 0.5 mm to 2.5 mm, in 0.5 mm
32 increments. When measured with a set of calipers, the channel widths on the printed masks were
33 each ~0.1 mm wider than the nominal width. Two sample papers after silane coating and
34 oxygen/plasma treatment are shown in **Figure 4B and C** with dye (food coloring in water) added
35 to visualize the patterned area. These initial results indicated that dimensional control was better
36 with the TCMS-treated papers. On the TCMS paper (**Figure 4B**), the channels were well-
37 defined, with the shape of the pattern closing mimicking that of the mask. On the TCOS paper
38 (**Figure 4C**), the patterned area appeared to extend well beyond the boundaries defined by the
39 mask. Of note, the channels at the bottom of the feature were much wider than those on the
40 mask, and the two channels on the far left began to overlap. The better-defined features on the
41 TCMS-coated paper may be because surface methyl groups from TCMS are easier to oxidize
42 more uniformly than the surface octyl groups from TCOS, or that the TCMS coating is more
43 uniform and/or denser prior to patterning. TCMS might not only be denser on the paper surface
44 but may also penetrate deeper into the fibrous structure of the paper. From these initial results,
45 we chose to further optimize channel dimensions with TCMS-coated paper substrates.
46
47
48
49

50
51 After selecting TCMS as the coating agent for our filter paper substrates (50 mM in
52 hexane for 5 min), we optimized dimensional control by exploring mask thickness,
53 oxygen/plasma intensity, and time exposed to oxygen/plasma treatment. We made multiple
54 masks similar to that in **Figure 4** with thicknesses varying from 1 to 3 mm. Measured channel
55 width on the paper as a function of mask channel width is shown for the 2-mm thick mask in
56
57
58
59
60

1
2
3 **Figure 5.** Graphs for other mask thicknesses are provided in the Electronic Supplementary
4 Information (Figures S1-S4). Food coloring in water was added to the patterned substrate, and
5 the widths of the colored regions were measured using calipers. Each data point on the graph is
6 an average of three measurements from three separate patterned substrates, and the error bars
7 represent the standard deviation of these measurements. We tested three intensities (low,
8 medium, high) and three exposure times (5, 10, 20 s). The black dashed-dotted line represents
9 the target channel widths, and the points and error bars represent channel widths measured from
10 3 different paper substrates after the addition of dye. For this mask, no channels were formed
11 under low intensity for 5 s, and only the 2.5-mm channel formed under low intensity for 10 s.
12 Several conditions resulted in channel widths close to the targets: low (20 s), medium (5 and
13 10 s), and high (5 s). Under high and medium intensities for longer times, the papers were
14 overexposed and had measured channel widths much larger than the targets. As expected,
15 measured channel width was a function of all three variables. In general, a thicker mask and
16 lower intensity required longer optimal exposure times. For example, the optimal intensity and
17 exposure times for the 3-mm thick mask (**Figure S4**) were medium for 10 s and high for 5 s, and
18 no channels were formed under low intensity (up to 20 s exposure). In contrast, the optimal
19 intensity and exposure times for the 1-mm thick mask (**Figure S1**) were low for 10 or 20 s and
20 medium for 5 s.
21
22
23
24
25

26
27 Triangular paper substrates for paper spray required slightly different patterning
28 parameters for optimal channel widths compared to the larger substrate, but the trends from the
29 larger substrates provided a useful starting point. A picture showing each of the masks for the
30 paper triangles is shown in **Figure 6A**. **Figure 6B** shows coated and patterned paper triangles for
31 each of the target channel widths (with dye added for visualization). Optimum conditions for
32 each channel width are shown in **Table S1**. The optimum time of exposure varied, but low
33 intensity was used in all cases. While similar channels could sometimes be generated between
34 low, medium, and high intensities, dimensional control tended to be more consistent with lower
35 intensities.
36
37

38
39 Before performing paper spray mass spectrometry, the effect of solvent composition on
40 observed channel width on the paper was investigated. Varying mixtures of water and methanol
41 from 95/5 (methanol/water, v/v) to 0/100 (methanol/water, v/v) were tested. Previous studies
42 with wax and paraffin barriers on paper substrates have been used with methanol content up to
43 80% with wax barriers^{44,46} and up to 100% with paraffin.⁴⁵ Sample papers spotted with these
44 mixtures in 5% composition increments are shown in **Figure S5**. More polar solvent ratios were
45 expected to be contained more within the channels, and that was the trend observed. At room
46 temperature, the channels became undefined above about 50% methanol. Interestingly, we
47 observed a temperature effect when testing the solvent composition. In **Figure S5A**, the channels
48 with solvent added are shown immediately after mixing, and the exothermic mixing of water and
49 methanol resulted in an elevated solvent temperature. In **Figure S5B**, the solvents were left to sit
50 on the bench overnight and then added to the papers. In **Figure S5C**, the solvents were stored in
51 the fridge overnight at 4 °C and then added to the papers. At higher solvent temperatures, the
52 channels became less defined at lower ratios of the methanol water mixture. At lower
53 temperatures, the channels remained more defined up to about 50% methanol. This observation
54
55
56
57
58
59
60

1
2
3 may be due to lower solvent viscosity at higher temperatures, which could enable the solvent to
4 spread more easily on the surface of the paper. We chose to use cold 50/50 methanol/water for
5 all our experiments to ensure the best definition of the filled channels possible while maintaining
6 maximum organic content.
7

8 *Paper Spray Mass Spectrometry*

9
10 We generated calibration curves for each of the four ARVs analyzed for patterned paper
11 substrates at each channel width as well as uncoated paper substrates. Sample calibration curves
12 comparing substrates with 2-mm channels to uncoated substrates are shown in **Figure 7**. Sample
13 MS/MS spectra for each analyte are shown in **Figure 8**. Calibration curves for the other channel
14 widths tested can be found in the electronic supplementary information (Figures S6-S9). The x-
15 axis for each calibration plot shows the concentration in ng/mL and the y-axis shows the ratio of
16 the area of the analyte peak (A) to the area of the internal standard peak (IS). Error bars represent
17 the standard error of three replicate paper substrates. For each of the analytes and channel widths
18 tested, the sensitivity (slope of the curve) was greater for all patterned papers versus the uncoated
19 papers. The increases in slope over uncoated substrates ranged from 2.5-fold up to 19-fold, with
20 an average increase of 7.2-fold across all channel widths and drugs tested. Every channel width
21 showed an improvement in sensitivity for every drug, but it is worth noting that the improvement
22 varied depending on drug and channel width. Similar variation was observed in the limits of
23 detection and quantification.
24
25
26
27
28

29 The limits of detection (LODs) and limits of quantification (LOQs) for each drug and
30 type of paper substrate are shown in **Table 1**. LODs were calculated as $3\sigma_{\text{blank}}/m$ and LOQs as
31 $10\sigma_{\text{blank}}/m$, where σ_{blank} was the standard deviation of the blank and m was the slope of the
32 calibration curve. Every channel width for the patterned papers showed improved LODs and
33 LOQs over the uncoated paper substrates. In the case of FTC analyzed with the uncoated papers,
34 the highest calibration level (1250 ng/mL) was below the LOQ (2200 ng/mL) and was the only
35 calibration level above the LOD (670 ng/mL). For comparison, the highest LOQ was 200 ng/mL
36 for the patterned papers, and the lowest was 24 ng/mL. The increase in sensitivity and
37 improvements in LOD/LOQ are likely due to multiple factors. First, the patterned papers
38 required lower volumes of solvent to sustain a stable electrospray for the time required to collect
39 the mass spectra (<10 μL for patterned vs 20 μL for uncoated). This results in a smaller dilution
40 factor – and therefore higher concentration – for the analytes after extraction for the patterned
41 paper substrates. Second, the pattern of the substrates directs all the solvent and sample toward
42 the mass spectrometer, likely resulting in more efficient delivery of analytes compared to
43 uncoated papers. In the case of the uncoated papers, both analyte and solvent spread throughout
44 the entirety of the surface of the substrate. Finally, there may be changes in spray dynamics, fluid
45 flow rate, or ionization efficiency that improve detection. These will be the subject of future
46 work.
47
48
49
50
51

52 In general, the detection limits from lowest to highest at a given channel width were:
53 DTG, 3TC, EFV, and FTC. The difference in detection limits is probably due to a combination
54 of physicochemical properties of the antiretrovirals studied and their interactions with the paper
55 substrates and solvent. For example, 3TC is the most polar of the drugs studied ($\log P = -1.4$), and
56
57
58
59
60

1
2
3 EFV is the most nonpolar ($\log P = 4.6$). DTG ($\log P = 2.2$) and FTC ($\log P = -0.4$) have polarities
4 between those two. Thus, the observed trend in detection limits cannot be explained by polarity
5 alone. Similarly, the trend cannot be explained only by mass (DTG > EFV > FTC > 3TC) or
6 basicity (EFV > DTG > FTC > 3TC). We plan to continue investigating these trends.
7
8

9 Interestingly, within a drug type, there was no clear trend in channel width versus
10 LOD/LOQ for any of the drugs tested here. The analysis of EFV with the 2-mm channel width
11 substrates showed higher LOD/LOQ than the other patterned papers, and the lowest LOD/LOQ
12 for EFV was observed with the 0.5-mm channel patterned papers. This observation was not
13 consistent across all analytes. The lowest LODs for 3TC and FTC were observed with the
14 2.5-mm patterned papers, and the lowest LOD for DTG was observed with the 1-mm patterned
15 papers. LODs and LOQs, as well as overall precision, would likely be improved with the use of
16 isotopically labeled internal standards.
17
18

19 *Detection of ARVs in Urine Samples*

20

21 After seeing the initial improvement of the patterning approach, we tested the
22 performance of our patterned substrates by spiking ARVs into human urine. We generated
23 calibration curves for each of the four ARVs using the 2-mm channel width paper substrates and
24 compared the results to uncoated paper substrates. The curves for each drug and substrate are
25 shown in **Figure 9**. The x-axis for each calibration curve shows the concentration in ng/mL and
26 the y-axis shows the ratio of the area of the analyte peak (A) to the area of the internal standard
27 peak (IS). Error bars represent the standard error of three replicate paper substrates. Similar to
28 the methanol/water matrix, a general improvement in sensitivity and LODs/LOQs was seen for
29 the patterned substrates over the uncoated substrates. The average improvement in sensitivity for
30 the patterned paper substrates was 7.4-fold, which was similar to that observed for the patterned
31 papers over the uncoated papers in the methanol/water matrix (7.2-fold). For FTC, EFV, and
32 DTG, the improvement in sensitivity ranged from 13-fold for FTC to 95-fold for DTG. For 3TC,
33 the patterned papers and uncoated papers showed similar sensitivities, with the sensitivity of the
34 patterned paper substrates approximately 60% of the sensitivity of the uncoated substrate. The
35 LODs and LOQs each of the ARVs in the urine samples are shown in **Table 2**. The patterned
36 paper substrates showed an improvement in LOD and LOQ for each of the four drugs, with an
37 average improvement of about 18-fold.
38
39
40
41
42

43 There was a predictable decrease in sensitivity and increase in LODs/LOQs when
44 switching from a neat matrix (methanol/water) to a biological matrix (urine) for the patterned
45 papers. For the uncoated paper substrates, many of the LODs were lower for urine than they
46 were for the neat matrix, despite lower sensitivity for all drugs. This change is due to lower
47 standard deviation of the blank samples, pointing to data collection with better reproducibility
48 than that of the methanol/water samples, which may be a result of more consistent non-zero
49 background from the more complex urine matrix. The changes in sensitivity and LODs for the
50 patterned papers are expected and likely due to ion suppression from the presence of salts and
51 other interfering compounds, commonly seen with paper spray mass spectrometry.^{6,11} Other
52 groups have attempted to overcome this limitation by changing solvents or performing a limited
53
54
55
56
57
58
59
60

1
2
3 amount of sample preparation (i.e. extraction).^{11,54–56} These and other strategies will be a focus
4 for improving sensitivity and LODs for our methods in the future.
5

6 **Conclusion**

7
8 In this study, we present a method for coating and patterning paper substrates for PS-MS.
9 Papers were modified using silane reagents to produce a hydrophobic coating before patterning a
10 hydrophilic channel via 3D-printed masks and surface oxidation with oxygen/plasma exposure.
11 TCMS and TCOS were initially chosen as primary coating agents as they produced optimal
12 coating parameters. Coating time, surface morphology, and hydrophobicity of the papers were
13 characterized using SEM, EDS, and CAG. TCMS was found to provide better dimensional
14 control over the patterned papers as demonstrated through the more defined filled channels on
15 TCMS-treated papers than TCOS-treated papers. Optimal intensity and exposure times were
16 developed for paper spray substrates with channels ranging from 0.5 to 2.5 mm in width. Solvent
17 composition was also studied, and we found that cold 50/50 methanol/water produced the most
18 defined channel while maintaining maximum organic content. PS-MS was performed to detect
19 four different ARVs for all five channel widths. Improved sensitivity, LOD, and LOQ were
20 observed for each of the patterned substrates compared to the uncoated substrates. Spiked urine
21 samples were analyzed by PS-MS with uncoated and a 2-mm patterned substrate. The patterned
22 substrates showed improved in sensitivity for three of the four target drugs and improved LOD
23 and LOQ for all of the target drugs. Future work will include exploration of other channel
24 geometries as well as sample preparation and analysis strategies for improved detection in
25 biological matrices.
26
27
28
29
30

31 **Conflicts of Interest**

32
33 The authors declare no potential conflicts of interest.
34

35 **Acknowledgements**

36
37 Research reported in this publication was supported by the National Institute of General Medical
38 Sciences of the National Institutes of Health under Award Number P20GM103499. The content
39 is solely the responsibility of the authors and does not necessarily represent the official views of
40 the National Institutes of Health.
41

42 This material is based upon work supported by the National Science Foundation under Grant No.
43 CHE-1757706.
44

45
46 The authors also gratefully acknowledge the Furman University Office of Undergraduate
47 Research and Furman University start-up funds.
48

49 **Author Contributions**

50
51 Austin Arias coated paper substrates, explored optimum solvent composition, optimized
52 patterning for one of the channel widths studied, and produced calibration curve and MS/MS
53 figures. Peyton Windham optimized patterning parameters for most of the channel widths,
54 produced most of the substrates for calibration experiments, performed the initial experiments
55 with ARVs in urine, and created the LOD/LOQ tables and figure with paper triangles and masks.
56
57
58
59
60

1
2
3 Natalie Cheyne performed coating experiments and measured contact angles. Mac Gilliland
4 collected most of the SEM and EDS data in the article and performed the calibration curve
5 experiments in the lab.
6
7
8
9
10
11
12
13
14
15
16
17
18
19
20
21
22
23
24
25
26
27
28
29
30
31
32
33
34
35
36
37
38
39
40
41
42
43
44
45
46
47
48
49
50
51
52
53
54
55
56
57
58
59
60

Figures and Tables

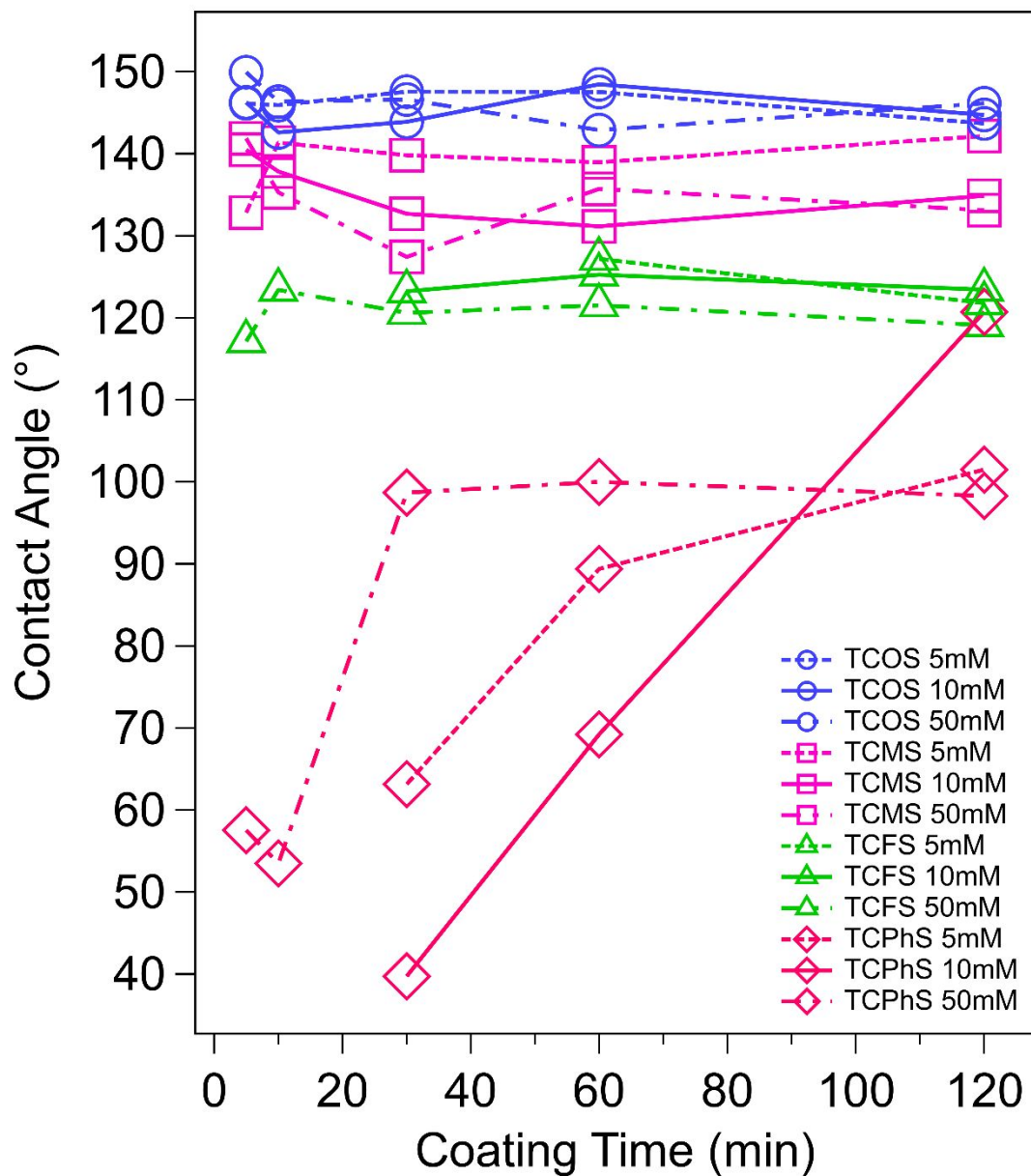


Figure 1. Contact angle as a function of coating time and silane concentration for paper substrates coated with four silanes: trichloromethyl silane (TCMS), trichlorophenylsilane (TCPhS), trichlorooctylsilane (TCOS), and trichloro-(3,3,3-trifluoropropyl)-silane (TCFS).

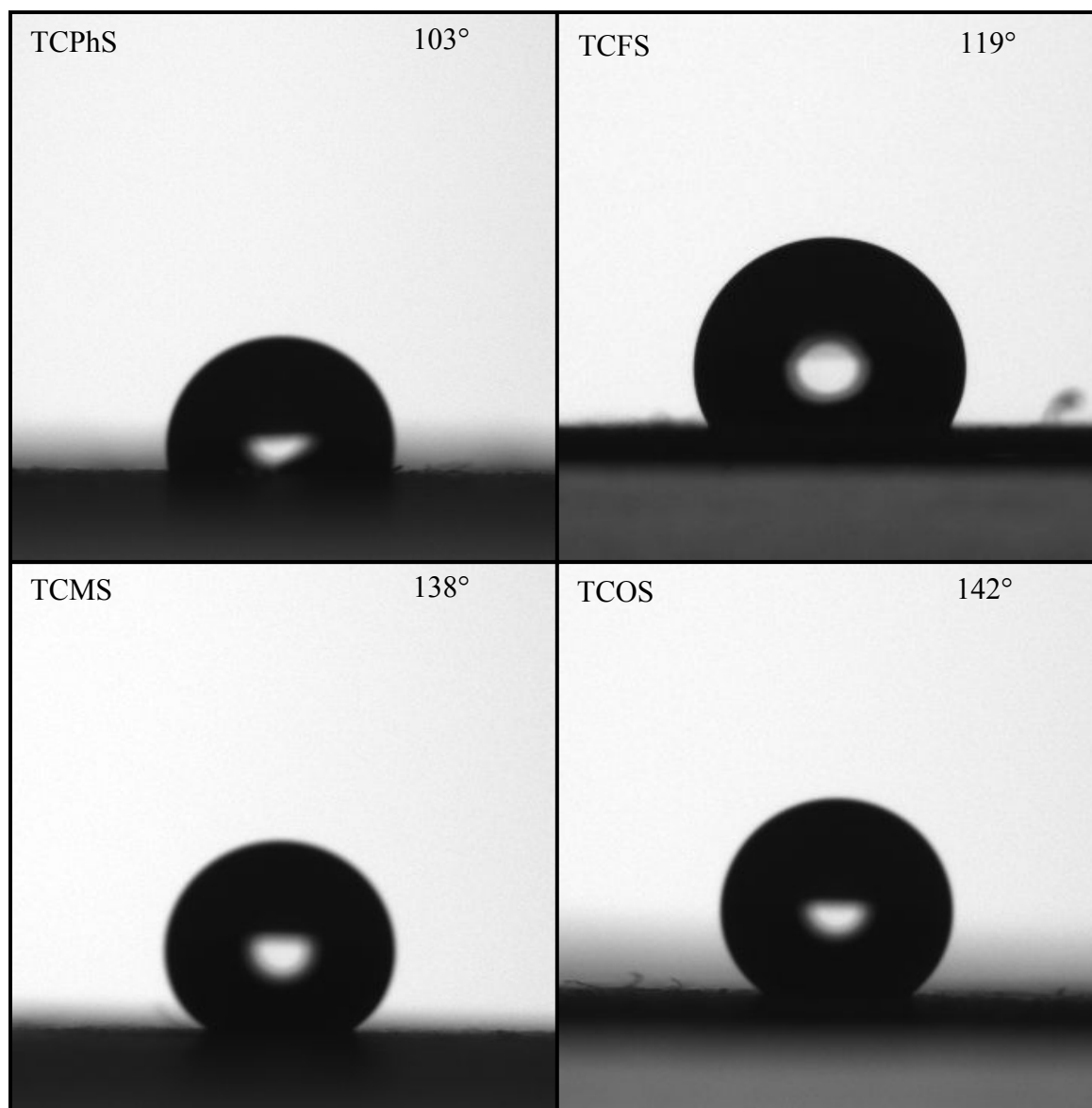


Figure 2. Sample contact angle images and angles for paper substrates coated with TCPhS, TCFS, TCMS, and TCOS. Each of the images was collected after immersing the papers for 2 h in 50 mM of their respective silanes.

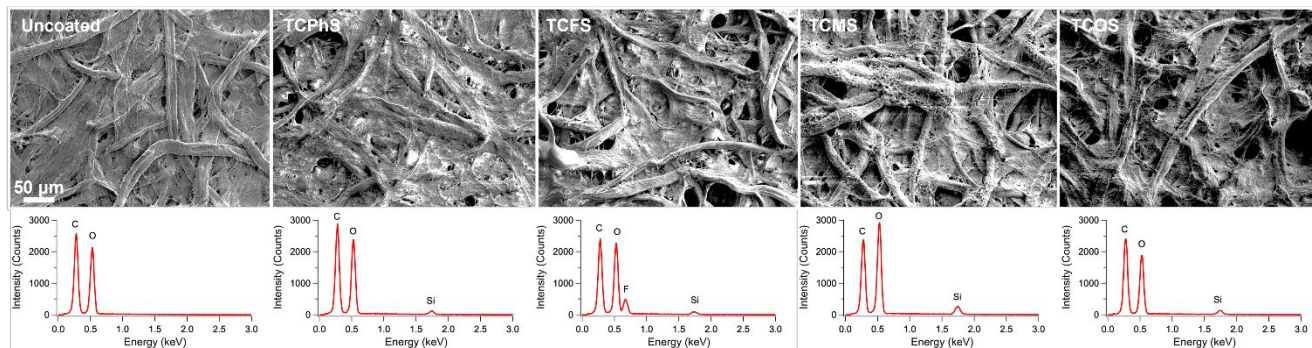


Figure 3. SEM images for an uncoated paper substrate and paper substrates coated with 50 mM of each silane for two hours (top) with corresponding EDS spectra (bottom). All SEM images were collected at 300x magnification and a probe current of 38.0 with the secondary electron detector. The beam voltage was 1.5 kV for the uncoated paper and was 2.0 kV for all of the coated papers.

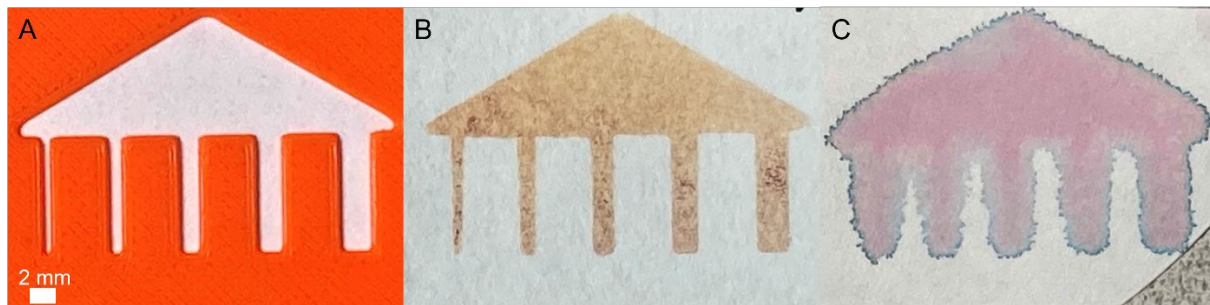


Figure 4. A) Sample mask made in orange plastic. B) Paper coated with TCMS and patterned with oxygen plasma, with dye added to visualize the channels. C) Paper coated with TCOS and patterned with oxygen plasma, with dye added to visualize the channels.

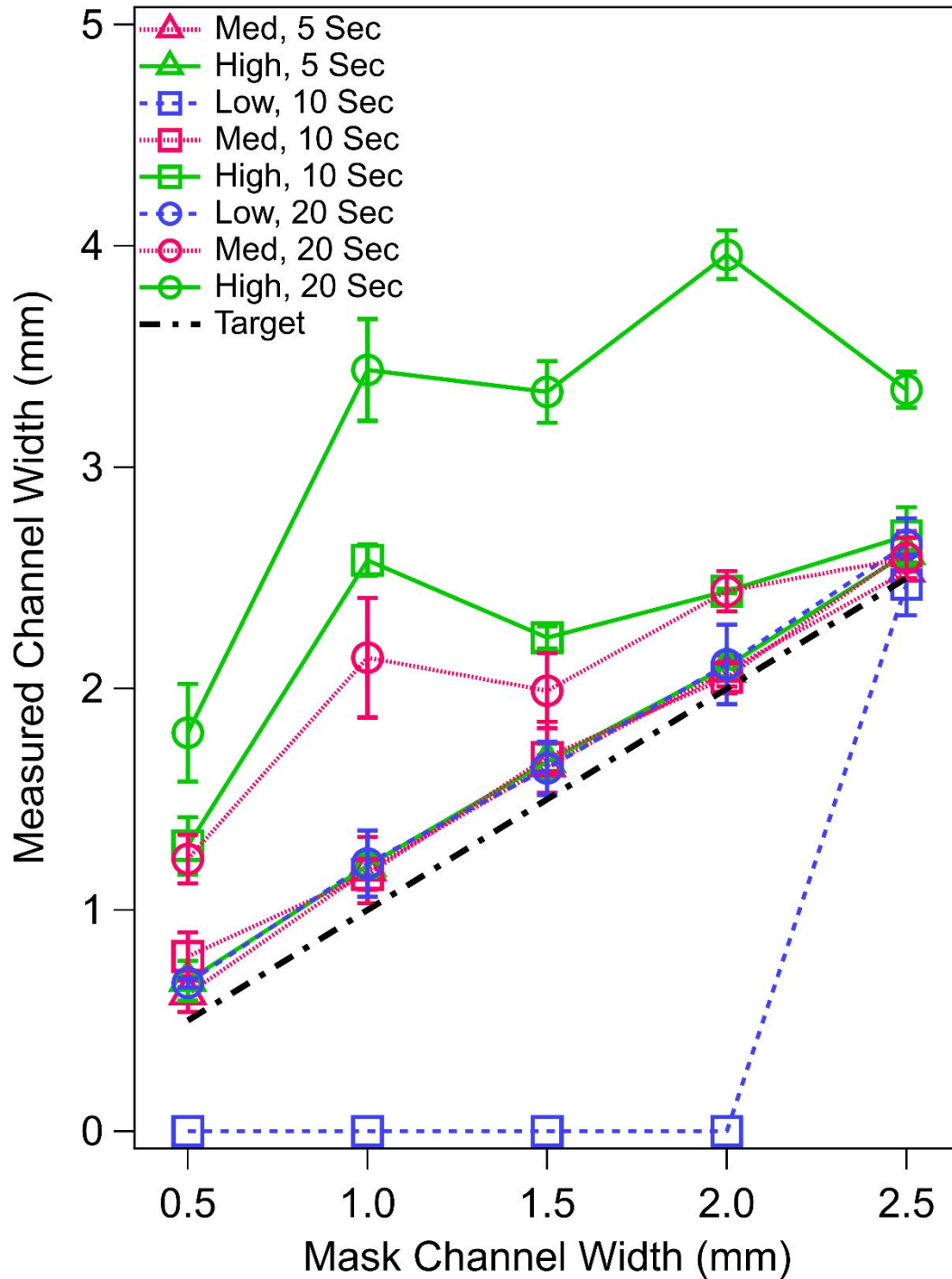


Figure 5. Measured channel width as a function of mask channel width for a 2-mm thick mask for 8 different oxygen plasma conditions from papers coated with 50 mM TCMS for 5 min. The dashed line indicated the target channel width. No channels were formed when the plasma cleaner was set at low for 5 seconds.

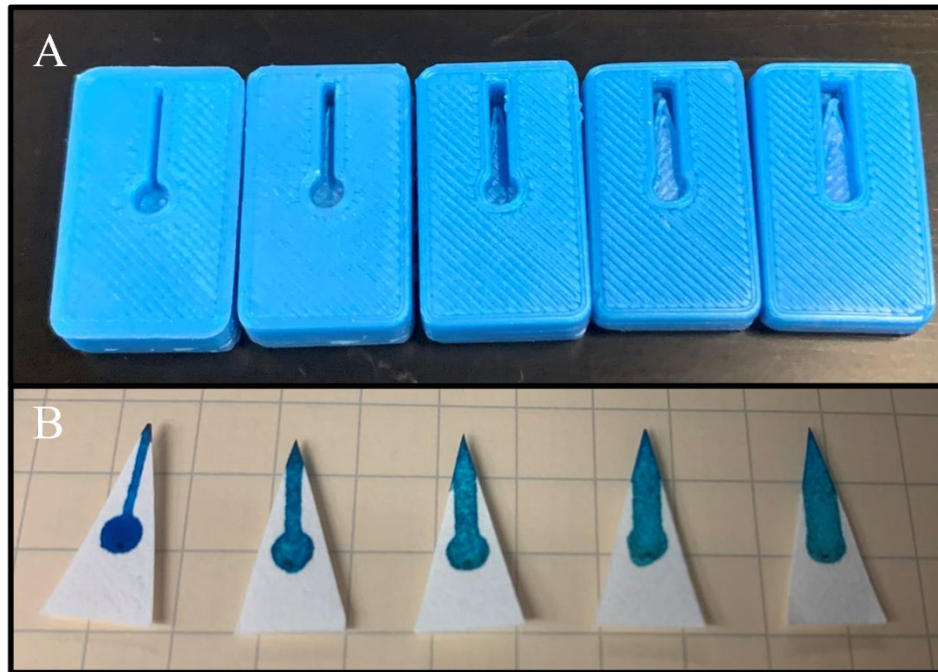


Figure 6. A) 3D-printed masks made from PLA for each channel width, ranging from 0.5 mm to 2.5 mm, shown in 0.5-mm increments from left to right. The outer dimensions of the masks are 15x25 mm. B) Paper substrates corresponding to the masks above, coated with TCMS (50 mM in hexane, 5 min) and patterned via oxygen/plasma with dye added to visualize the channels. The paper dimensions are 8 x 16 mm (base x height).

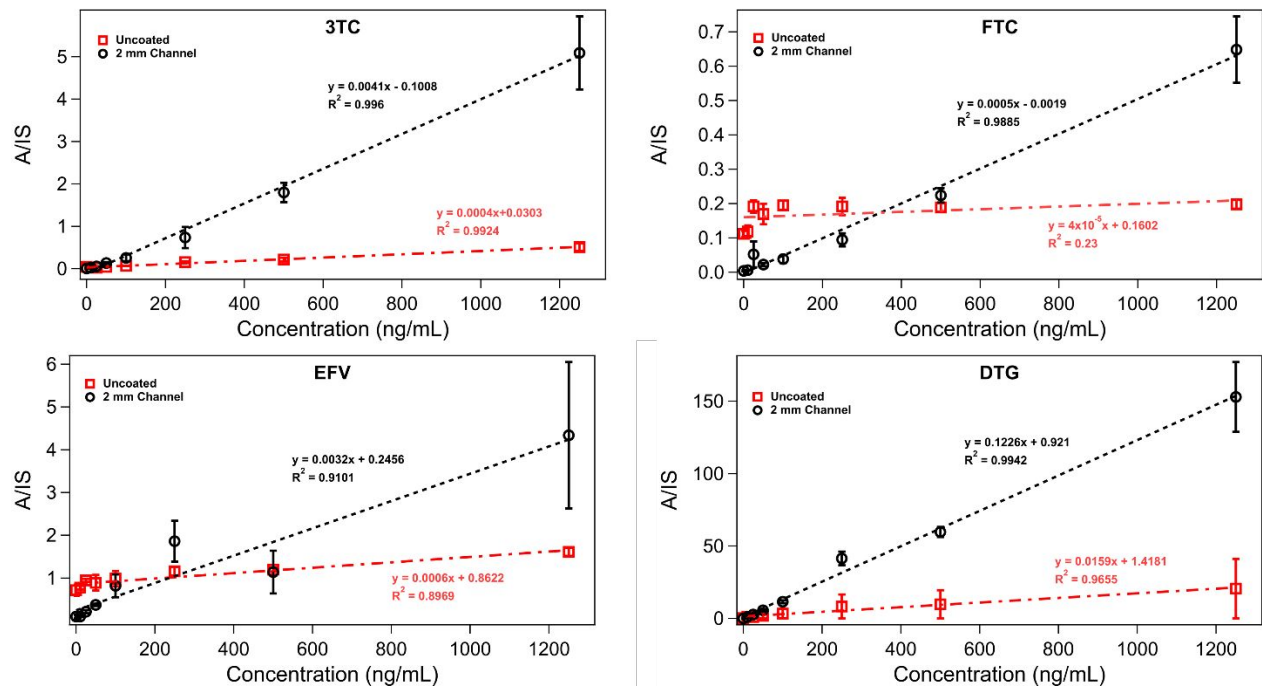


Figure 7. Calibration curves for uncoated (red squares) and patterned papers with 2-mm channels (black circles) for four target antiretrovirals in methanol/water. The y-axis is the area of the analyte peak (A) divided by the area of the internal standard peak (IS). The error bars represent the standard error of 3 measurements.

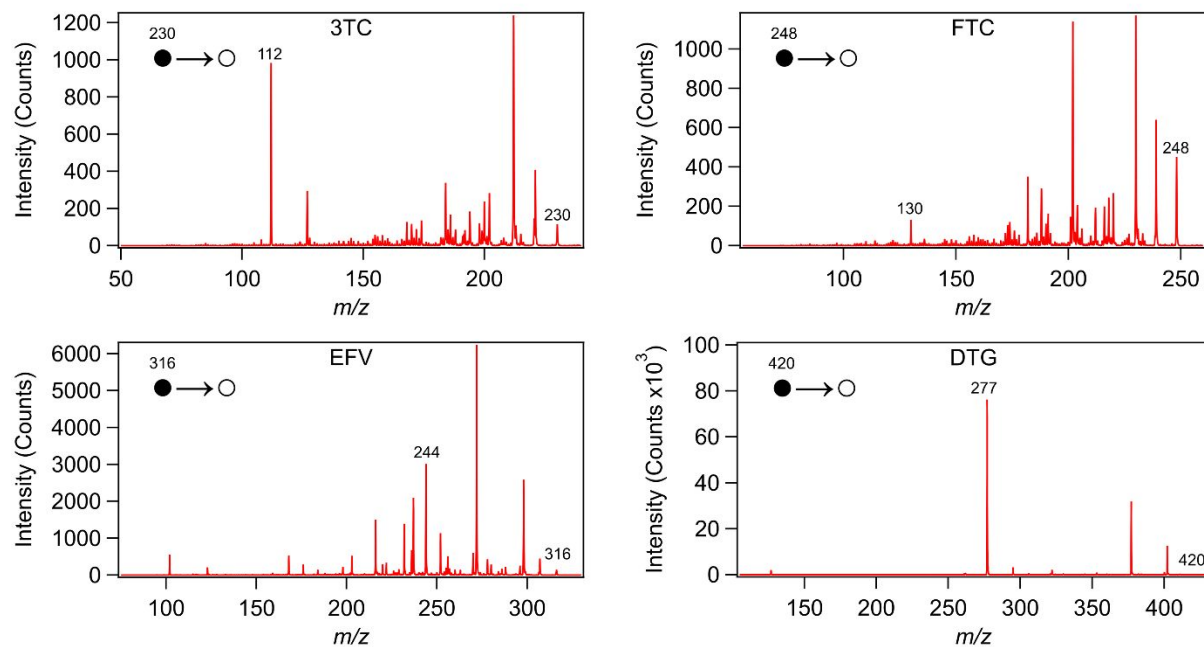


Figure 8. Sample MS/MS spectra for each of the four antiretrovirals analyzed in the study. The spectrum for each drug is labeled accordingly: lamivudine (3TC), emtricitabine (FTC), efavirenz (EFV), and dolutegravir (DTG). Precursor and product ions for each drug are labeled in the figure.

Table 1. Limits of detection and quantification for each drug and channel width examined in methanol/water.

Channel Widths (mm)	Drug Type							
	3TC		FTC		EFV		DTG	
	LOD	LOQ	LOD	LOQ	LOD	LOQ	LOD	LOQ
Uncoated	160	550	670	2200	620	2100	9.8	33
0.5	0.77	2.6	14	48	1.8	6.0	0.10	0.34
1	1.8	6.1	59	200	4.1	14	0.014	0.048
1.5	1.9	6.5	60	200	3.1	10	0.019	0.062
2	1.8	5.8	7.2	24	42	140	0.076	0.25
2.5	0.28	0.92	11	36	2.1	7.1	0.17	0.58

LOD: limit of detection, calculated as $3\sigma_{blank}/m$; LOQ: limit of quantification, calculated as $10\sigma_{blank}/m$
All LODs and LOQs are reported in units of ng/mL

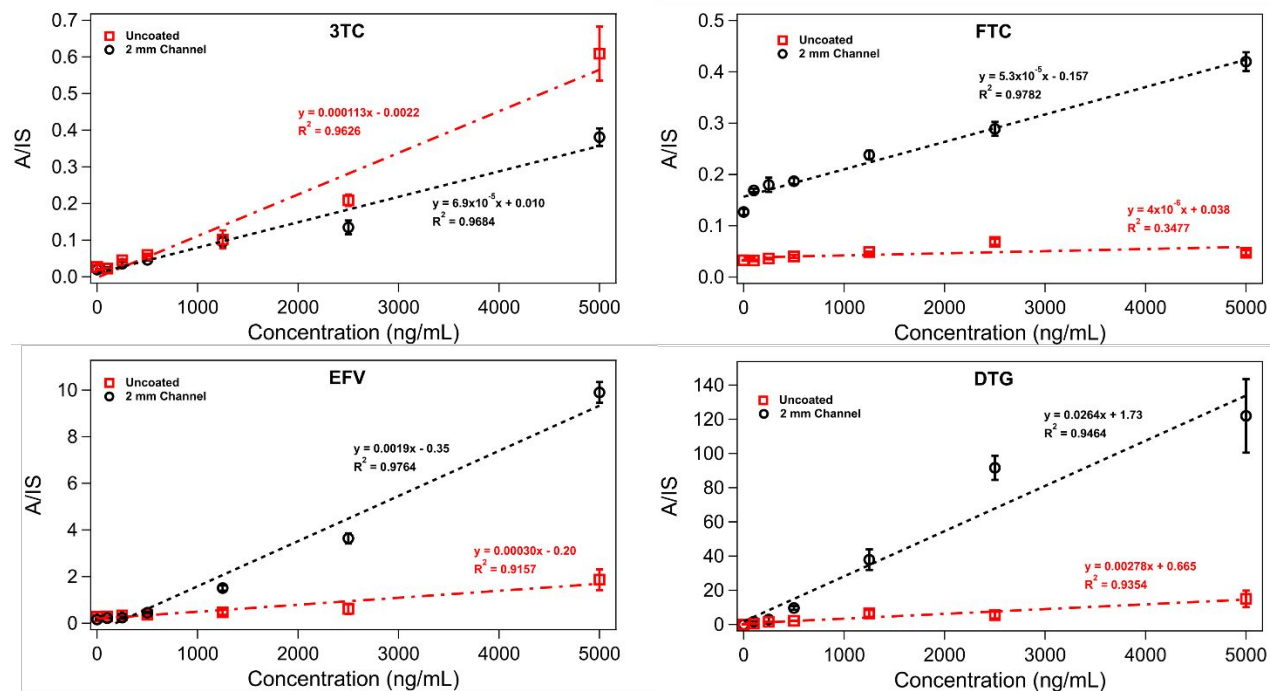


Figure 9. Calibration curves for uncoated (red squares) and patterned papers with 2-mm channels (black circles) for four target antiretrovirals spiked in urine. The y-axis is the area of the analyte peak (A) divided by the area of the internal standard peak (IS). The error bars represent the standard error of 3 measurements.

Table 2. Limits of detection and quantification for each drug and channel width examined in urine.

Channel Widths (mm)	Drug Type							
	3TC		FTC		EFV		DTG	
	LOD	LOQ	LOD	LOQ	LOD	LOQ	LOD	LOQ
Uncoated	165	551	424	1410	129	430	9.9	33
2	86.8	289	307	1020	4.3	14	0.25	0.84

*LOD: limit of detection, calculated as $3\sigma_{blank}/m$; LOQ: limit of quantification, calculated as $10\sigma_{blank}/m$
All LODs and LOQs are reported in units of ng/mL*

References

- 1 C. L. Feider, A. Krieger, R. J. Dehoog and L. S. Eberlin, *Anal Chem*, 2019, **91**, 4266–4290.
- 2 T. H. Kuo, E. P. Dutkiewicz, J. Pei and C. C. Hsu, *Anal Chem*, 2020, **92**, 2353–2363.
- 3 Z. Takáts, J. M. Wiseman, B. Gologan and R. G. Cooks, *Science (1979)*, 2004, **306**, 471–473.
- 4 R. G. Cooks, Z. Ouyang, Z. Takats and J. M. Wiseman, *Science (1979)*, 2006, **311**, 1566–1570.
- 5 R. B. Cody, J. A. Laramée and H. D. Durst, *Anal Chem*, 2005, **77**, 2297–2302.
- 6 H. Wang, J. Liu, R. Graham Cooks and Z. Ouyang, *Angewandte Chemie International Edition*, 2010, **49**, 877–880.
- 7 C. B. Nguyen, W. R. A. Wichert, D. O. Carmany, E. M. McBride, P. M. Mach, E. S. Dhummakupt, T. Glaros and N. E. Manicke, *Anal Chem*, 2021, **93**, 13467–13474.
- 8 E. S. Dhummakupt, D. O. Carmany, P. M. Mach, T. M. Tovar, A. M. Ploskonka, P. S. Demond, J. B. DeCoste and T. Glaros, *ACS Appl Mater Interfaces*, 2018, **10**, 8359–8365.
- 9 A. E. O’Leary, S. E. Hall, K. E. Vircks and C. C. Mulligan, *Analytical Methods*, 2015, **7**, 7156–7163.
- 10 P. W. Fedick, B. J. Bills, N. E. Manicke and R. G. Cooks, *Anal Chem*, 2017, **89**, 10973–10979.
- 11 E. L. Rossini, D. S. Kulyk, E. Ansu-Gyeabourh, T. Sahraeian, H. R. Pezza and A. K. Badu-Tawiah, *J Am Soc Mass Spectrom*, 2020, **31**, 1212–1222.
- 12 C. J. Pulliam, R. M. Bain, J. S. Wiley, Z. Ouyang and R. G. Cooks, *J Am Soc Mass Spectrom*, 2015, **26**, 224–230.
- 13 S. L. Reeber, S. Gadi, S. ben Huang and G. L. Glish, *Analytical Methods*, 2015, **7**, 9808–9816.
- 14 S. Maher, F. P. M. Jjunju, D. E. Damon, H. Gorton, Y. S. Maher, S. U. Syed, R. M. A. Heeren, I. S. Young, S. Taylor and A. K. Badu-Tawiah, *Scientific Reports 2016 6:1*, 2016, **6**, 1–10.
- 15 F. P. M. Jjunju, S. Maher, D. E. Damon, R. M. Barrett, S. U. Syed, R. M. A. Heeren, S. Taylor and A. K. Badu-Tawiah, *Anal Chem*, 2016, **88**, 1391–1400.
- 16 S. Maher, F. P. M. Jjunju, D. E. Damon, H. Gorton, Y. S. Maher, S. U. Syed, R. M. A. Heeren, I. S. Young, S. Taylor and A. K. Badu-Tawiah, *Scientific Reports 2016 6:1*, 2016, **6**, 1–10.
- 17 I. Mahmud, F. G. Pinto, V. Y. Rubio, B. Lee, C. P. Pavlovich, R. J. Perera and T. J. Garrett, *Anal Chem*, 2021, **93**, 7774–7780.
- 18 J. A. Michely, M. R. Meyer and H. H. Maurer, *Anal Chem*, 2017, **89**, 11779–11786.
- 19 C. Zhang and N. E. Manicke, *Anal Chem*, 2015, **87**, 6212–6219.
- 20 R. Jett, C. Skaggs and N. E. Manicke, *Analytical Methods*, 2017, **9**, 5037–5043.
- 21 S. Chiang, W. Zhang and Z. Ouyang, *Expert Rev Proteomics*, 2018, **15**, 789.
- 22 S. Chen, Q. Wan and A. K. Badu-Tawiah, *J Am Chem Soc*, 2016, **138**, 6356–6359.
- 23 N. E. Manicke, Q. Yang, H. Wang, S. Oradu, Z. Ouyang and R. G. Cooks, *Int J Mass Spectrom*, 2011, **300**, 123–129.

- 1
2
3 24 J. V. Coelho Pimenta, R. Augusti and A. A. Sabino, *J Am Soc Mass Spectrom*, 2021, **32**,
4 2168–2174.
5
6 25 X. Zhou, J. Pei and G. Huang, *Rapid Communications in Mass Spectrometry*, 2015, **29**,
7 100–106.
8
9 26 D. Sarkar, A. Som and T. Pradeep, *Anal Chem*, 2017, **89**, 11378–11382.
10 27 S. Banerjee, C. Basheer and R. N. Zare, *Angewandte Chemie International Edition*, 2016,
11 **55**, 12807–12811.
12 28 R. M. Bain, C. J. Pulliam, S. A. Raab and R. G. Cooks, *J Chem Educ*, 2016, **93**, 340–344.
13 29 J. Li, Y. Zheng, W. Mi, T. Muyizere and Z. Zhang, *Analytical Methods*, 2018, **10**, 2803–
14 2811.
15 30 T. Wang, Y. Zheng, X. Wang, D. E. Austin and Z. Zhang, *Anal Chem*, 2017, **89**, 7988–
16 7995.
17
18 31 Y. Zheng, Q. Wang, X. Wang, Y. Chen, X. Wang, X. Zhang, Z. Bai, X. Han and Z.
19 Zhang, *Anal Chem*, 2016, **88**, 7005–7013.
20 32 Y. Zheng, X. Zhang, H. Yang, X. Liu, X. Zhang, Q. Wang and Z. Zhang, *Analytical*
21 *Methods*, 2015, **7**, 5381–5386.
22
23 33 Q. Wang, Y. Zheng, X. Zhang, X. Han, T. Wang and Z. Zhang, *Analyst*, 2015, **140**, 8048–
24 8056.
25 34 P. W. Fedick, F. Pu, N. M. Morato and R. G. Cooks, *J Am Soc Mass Spectrom*, 2020, **31**,
26 735–741.
27
28 35 D. S. Burr, W. L. Fatigante, J. A. Lartey, W. Jang, A. R. Stelmack, N. W. McClurg, J. M.
29 Standard, J. R. Wieland, J. H. Kim, C. C. Mulligan and J. D. Driskell, *Anal Chem*, 2020,
30 **92**, 6676–6683.
31
32 36 X. Wang, Y. Zheng, T. Wang, X. Xiong, X. Fang and Z. Zhang, *Analytical Methods*,
33 2016, **8**, 8004–8014.
34 37 E. S. Dhummakupt, D. O. Carmany, P. M. Mach, T. M. Tovar, A. M. Ploskonka, P. S.
35 Demond, J. B. DeCoste and T. Glaros, *ACS Appl Mater Interfaces*, 2018, **10**, 8359–8365.
36
37 38 P. Basuri, A. Baidya and T. Pradeep, *Anal Chem*, 2019, **91**, 7118–7124.
38 39 D. E. Damon, K. M. Davis, C. R. Moreira, P. Capone, R. Cruttenden and A. K. Badu-
39 Tawiah, *Anal Chem*, 2016, **88**, 1878–1884.
40 40 D. E. Damon, M. Yin, D. M. Allen, Y. S. Maher, C. J. Tanny, S. Oyola-Reynoso, B. L.
41 Smith, S. Maher, M. M. Thuo and A. K. Badu-Tawiah, *Anal Chem*, 2018, **90**, 9353–9358.
42
43 41 Z. Chen, Q. Shi, W. Wang, Z. Jiang, G. L. Zhang, L. Tong, X. Mu and B. Tang, *Anal*
44 *Chem*, 2021, **93**, 1749–1756.
45 42 J. Liu, Y. He, S. Chen, M. Ma, S. Yao and B. Chen, *Talanta*, 2017, **166**, 306–314.
46 43 T. Zargar, T. Khayamian and M. T. Jafari, *Microchimica Acta*, 2018, **185**, 1–9.
47 44 I. Murray, G. Walker and M. S. Bereman, *Analyst*, 2016, **141**, 4065–4073.
48 45 T. C. Colletes, P. T. Garcia, R. B. Campanha, P. V. Abdelnur, W. Romão, W. K. T. Coltro
49 and B. G. Vaz, *Analyst*, 2016, **141**, 1707–1713.
50
51 46 D. E. Damon, Y. S. Maher, M. Yin, F. P. M. Jjunju, I. S. Young, S. Taylor, S. Maher and
52 A. K. Badu-Tawiah, *Analyst*, 2016, **141**, 3866–3873.
53 47 S. Azizov, M. Sharipov, J. M. Lim, S. M. Tawfik, N. Kattaev and Y. I. Lee, *Journal of*
54 *Mass Spectrometry*, 2021, **56**, e4611.
55
56
57
58
59
60

- 1
2
3 48 S. Jackson, S. Lee and A. K. Badu-Tawiah, *Anal Chem*, 2022, **94**, 5132–5139.
4 49 Q. He, C. Ma, X. Hu and H. Chen, *Anal Chem*, 2013, **85**, 1327–1331.
5 50 M. Hashemi Hedeshi, O. Rezvani and H. Bagheri, *Anal Chim Acta*, 2020, **1128**, 31–41.
6 51 Y. Zhang, T. Ren and J. He, *ACS Appl Mater Interfaces*, 2018, **10**, 11343–11349.
7 52 FDA Drug Data, www.accessdata.fda.gov/, (accessed 30 August 2023).
8 53 P. Samyn, *Journal of Materials Science 2013 48:19*, 2013, **48**, 6455–6498.
9 54 S. A. Borden, A. Saatchi, J. Palaty and C. G. Gill, *Analyst*, 2022, **147**, 3109–3117.
10 55 F. M. de Oliveira, G. L. Scheel, R. Augusti, C. R. T. Tarley and C. C. Nascentes, *Anal*
11 *Chim Acta*, 2020, **1106**, 52–60.
12 56 Y. Yang, J. Wu, J. Deng, K. Yuan, X. Chen, N. Liu, X. Wang and T. Luan, *Anal Chim*
13 *Acta*, 2018, **1032**, 75–82.
14
15
16
17
18
19
20
21
22
23
24
25
26
27
28
29
30
31
32
33
34
35
36
37
38
39
40
41
42
43
44
45
46
47
48
49
50
51
52
53
54
55
56
57
58
59
60